Research Article

Avinash Shinde, Irulappasamy Siva*, Yashwant Munde, Irulappasamy Sankar, Mohamed Thariq Hameed Sultan*, Farah Syazwani Shahar, Milan Gaff*, and David Hui

Appraising the dielectric properties and the effectiveness of electromagnetic shielding of graphene reinforced silicone rubber nanocomposite

https://doi.org/10.1515/ntrev-2022-0558
received March 7, 2023; accepted May 15, 2023

Abstract: The aim of this research is to measure the dielectric properties and electromagnetic interference (EMI) shielding effectiveness (SE) of silicone rubber reinforced with graphene nanoplates. In a two-roll mill, different amounts of graphene are mixed together. This is followed by compression moulding at 170°C and post-curing for 4 h at 200°C. Between 1 MHz and 1 GHz, the waveguide transmission line method and a vector network analyser are used to measure the dielectric and EMI SE parameters. As the amount of graphene is increased from 0 to 7 wt%, AC conductivity goes up, reaching 1.19×10^{-3} S/cm at 7 wt%. The same composition gives the highest EMI SE of 43.22 dB at 1 GHz. The high-frequency structural simulation of different compositions shows how shielding works, and the results agree with what has been seen in experiments.

Keywords: silicone rubber, graphene, nanocomposites, EMI SE, dielectric

*** Corresponding author: Irulappasamy Siva,** Department of Civil Engineering, Rajas Institute of Technology, Nagercoil, 629001, Tamilnadu, India; Center for Composite Materials, Kalasalingam Academy of Research and Education, Anand Nagar, 626126, TN, India, e-mail: isiva@klu.ac.in
*** Corresponding author: Mohamed Thariq Hameed Sultan,** Department of Aerospace Engineering, Faculty of Engineering, Universiti Putra Malaysia, UPM Serdang, Seri Kembangan 43400, Selangor Darul Ehsan, Malaysia; Laboratory of Bio-composite Technology, Institute of Tropical Forestry and Forest Products (INTROP), Universiti Putra Malaysia, Serdang, Seri Kembangan 43400, Selangor Darul Ehsan, Malaysia; Aerospace Malaysia Innovation Centre (944751-A), Prime Minister's Department, MIGHT Partnership Hub, Jalan Impact, Cyberjaya 63000, Selangor Darul Ehsan, Malaysia, e-mail: thariq@upm.edu.my
*** Corresponding author: Milan Gaff,** Faculty of Civil Engineering, Experimental Centre, Czech Technical University in Prague, Thakurova 7, 166 29 Prague 6, Czech Republic; Department of Furniture, Design and Habitat (FFWT), Mendel University in Brno, Zemědělská 1665, 613 00 Brno-sever-Černá Pole, Czech Republic, e-mail: gaffmilan@gmail.com
Avinash Shinde: Center for Composite Materials, Kalasalingam Academy of Research and Education, Anand Nagar, 626126, TN, India; Department of Mechanical Engineering, Cummins College of Engineering for Women, Pune, MH, India
Yashwant Munde: Department of Mechanical Engineering, Cummins College of Engineering for Women, Pune, MH, India
Irulappasamy Sankar: Department of Mechanical Engineering, National Engineering College, Kovilpatti, 628503, TN, India
Farah Syazwani Shahar: Department of Aerospace Engineering, Faculty of Engineering, Universiti Putra Malaysia, UPM Serdang, Seri Kembangan 43400, Selangor Darul Ehsan, Malaysia
David Hui: Department of Mechanical Engineering, University of New Orleans, New Orleans, Louisiana, United States of America

1 Introduction

The increasing use of electronic equipment in various industries, such as defence, aerospace, automotive, and even ordinary life, has led to massive electromagnetic (EM) radiation exposure. It is incomprehensible that online education and the work-from-home culture would have taken off in the post-covid era without computers, mobile phones, Wi-Fi, and other electronic devices [1]. When one electronic equipment sends erroneous or accidental electromagnetic (EM) signals that interfere with and impair the performance of another electronic device, this is known as electromagnetic interference (EMI). It may cause electrical implants in the human body to malfunction and pose health dangers [2,3]. However, our dependence on technological gadgets has reached such a level that abandoning them would be a "crazy fantasy." One possible approach is shielding sensitive electronics from EM radiation, also known as EMI shielding (EMI shielding).

Historically, various metals have been used for EMI shielding, but their limitations include their high

density, poor corrosion resistance, and high price [4]. Strong conductivity, lightweight, and good manufacturing capabilities are necessary for the EMI shielding material without sacrificing mechanical performance [5]. EMI shielding performance may be considerably improved by enhancing conductivity with a suitable filler [5]. Polymer composites with suitable fillers may be viable solutions for meeting these property specifications. Polymer is mixed with various fillers, including metals, carbon black, graphite, ferrite, and graphene.

Silicone rubber (SR), a low-density elastomer, is utilised in several applications due to its easy formability, chemical resistance, and weather resistance. Nonetheless, SR is an insulating material that EMI waves can easily pass through. Including conductive fillers increases SR's conductivity to attain the necessary EMI shielding properties. This conductive SR is commonly employed in EMI shielding applications [6]. Carbon black [7–9], carbon fibres [10,11], and graphene [9,12,13], are commonly used fillers in SR [13]. The conductivity of SR rises with an increase in filler percentage, resulting in better EMI shielding effectiveness (SE). Other varieties of SR, such as RTV, HTV, and PDMS, are also investigated.

Additionally, graphene is frequently used with different matrix materials to improve the conductivity of polymers. Bregman *et al.* [7] investigated the complex electromagnetic characteristics of graphene nanoplatelet reinforced in poly-lactic acid. The SR containing carbon and ferrite powder's EMI SE varies with frequency for samples with low conductivity. However, samples with high conductivity demonstrate consistent performance [14]. A 3D conductive structure made of silver nanowires and graphene oxides is created in the PDMS matrix using the hydrogel approach. This results in a 34.1 dB absorption-dominated EMI SE [15]. SR with magnetic microwires and graphene fibres improves SE by 18 dB. Ultrasonic mixing, and degassing produces a frequency-selective EMI SE material from SR (methyl vinyl) graphene. The EMI SE improves with an SE of 30.42 dB [16].

Literature analysis reveals that different production processes are utilised to manufacture various grades of graphene-coated SR. This research uses common rubber processing techniques. SR (SH5060U grade) and graphene nanocomposite are produced for EMI shielding applications. As a result, the developed nanocomposite is easily adaptable and practical for commercial use. It is reported that SR/graphene nanocomposite has complex dielectric properties and EMI SE. A simulation run on the Ansys high-frequency structural simulation (HFSS) software supports the findings.

2 Materials, manufacturing, and experimental details

2.1 Constituent material details

SR of grade SH5060U and the peroxide-based accelerator known as Di-Cup-40 are both supplied by Krupa Chemicals, Pune, India (dicumyl peroxide; DCP). A graphene sheet can have five to ten layers, 5–10 nm thick, and a typical lateral dimension of 10 nm. The material specifications are presented in Table 1.

2.2 Manufacturing details of composite

The graphene-based SR and DCP compound SRG1, SRG2, SRG3, SRG4, and SRG5 have varying graphene weight fractions 0, 1, 3, 5, and 7%, respectively. SRG1, SRG2, SRG3, SRG4, and SRG5 are the names given to these graphene weight fractions, respectively. Figure 1 depicts the manufacturing process, and Table 2 lists the filler and curing agent compositions used with SR. The procedure's first phase is used to combine the SR and graphene in a machine with two rolls. The compound is then moulded for 5 min at a moulding pressure of 50 bars using a compression moulding machine (make: SANTEC, capacity: 30 tonnes). The post-curing procedure takes place for 4 h at a temperature of 200°C in an oven with hot air (made by Athena Technology; the model number is ATAO-3S/G).

2.3 Experimental details

Several dielectric and EMI SE domains are tested using three distinct compositions, each with three samples. FESEM and FTIR investigations are also performed to confirm graphene dispersion and understand how the

Table 1: Material property details

Type/grade	SR (SH5060 U)	Graphene
Specific gravity (g/cc)	1.15	1.6
Tensile strength, ultimate	5 MPa	130 GPa
Elongation (%)	500	5
Hardness, shore	50 (A)	70 HRC

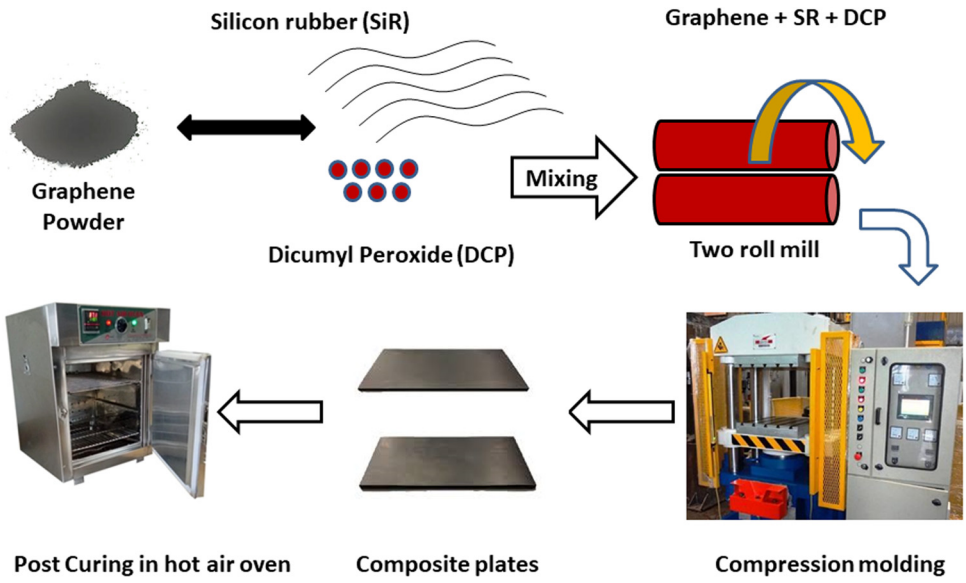

Figure 1: Schematic representation of the manufacturing process.

Table 2: Weight percentages of filler and curing agent

Type/grade	SRG1	SRG2	SRG3	SRG4	SRG5
Graphene	0	1	3	5	7
DCP	2	2	2	2	2

composite developed. The following sections will cover the specifics of each characterisation that was previously addressed. The images created by the scanning electron microscope (SEM) are captured using a VEGA 3TSCAN device with ultra-high resolution. The tool used for FTIR spectroscopy is a Shimadzu Miracle with ART.

2.4 EMI and dielectric analysis

On compression-moulded samples that were 1 mm thick, the waveguide transmission line method was utilised on a vector network analyser (VNA) (Agilent Technologies E5071C, ENA series, 1 MHz to 1 GHz, CA). The S_{11} and S_{12} scattering properties are measured, and the EMI SE is calculated. The built-in software uses the Nicolson–Ross–Weir (NRW) technique to estimate the dielectric characteristics with the scattering factors (S_{11} and S_{12}) as inputs. The S-parameters can be used to determine the components of reflection and absorption.

3 Results and discussion

3.1 Morphological characteristics

The microstructure of several SR/graphene mixes was examined using SEM. Figure 2 shows pictures taken with a SEM at 100× magnification. Due to the compositions' inability to be combined, distinct phases of SR and graphene may be seen in SR/graphene compositions. Figure 2 depicts the graphene dispersion in the rubber matrix (a–f). The weight percent of graphene is increasing in Figure 2. The pattern of surface ripples characterises the unique shape of graphene dispersion. The microstructure makes it simple to see how evenly the graphene particles are dispersed throughout the SR matrix.

Figure 3 shows the FTIR spectra for every possible mix of SR and graphene. These spectra show where silicone-containing groups are distributed. All samples can exhibit the fundamental functional group of SR at wavenumbers between 500 and 1,300 cm^{-1}. Si–O–Si stretching, Si–O of O–Si$(CH_3)_2$–O, and Si–CH_3 symmetry bending all reach their maximum values at 1,010, 789, and 1,257 cm^{-1}, respectively. The measured FTIR peak intensities experience a slight attenuation due to the presence of graphene. This result could be explained by the graphene barrier impeding the detection of Si chemical bonds in SR [17,18]. It was discovered that all samples included a

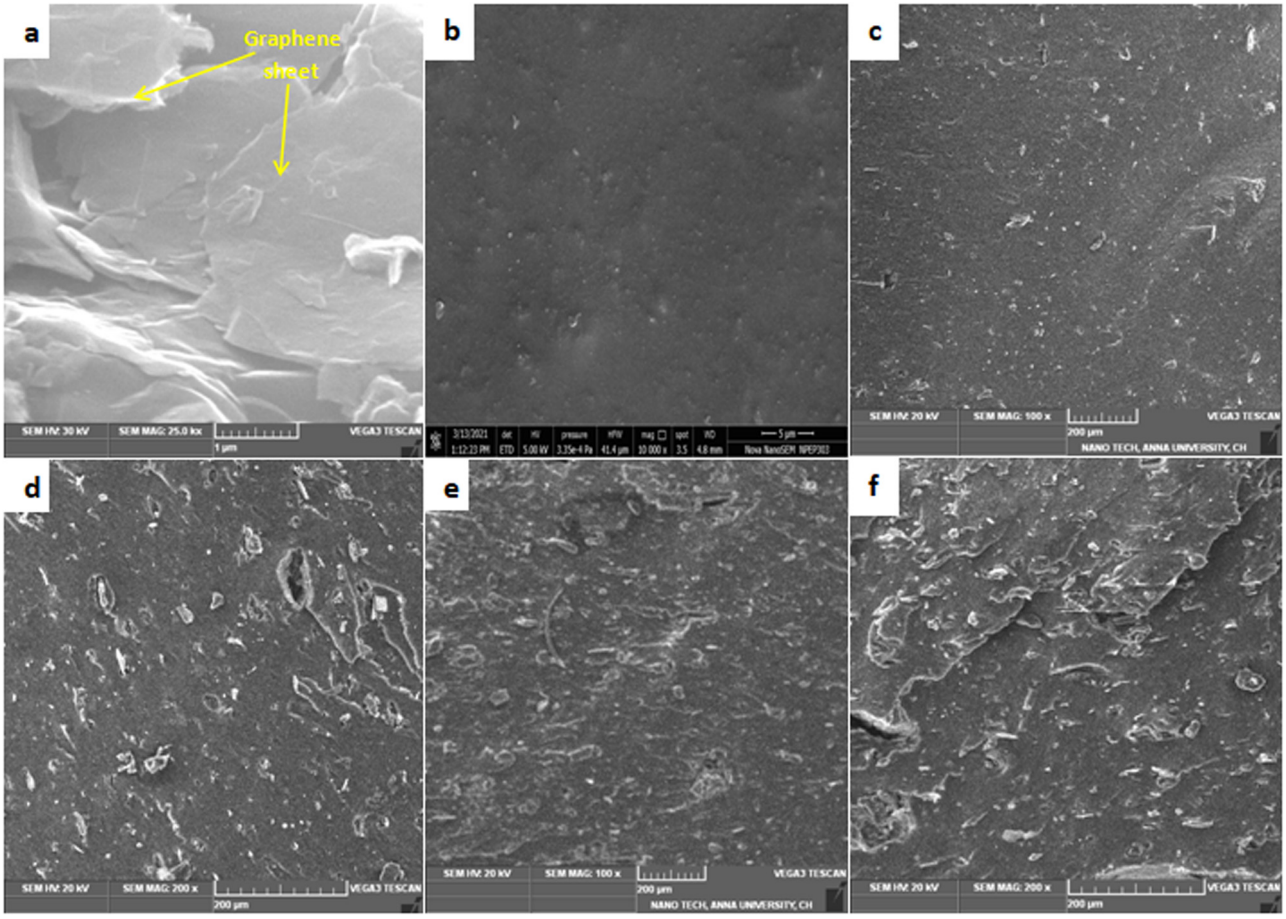

Figure 2: SEM micrographs of (a) graphene powder and surfaces of (b) SRG1, (c) SRG2, (d) SRG3, (e) SRG4, and (f) SRG5 composition.

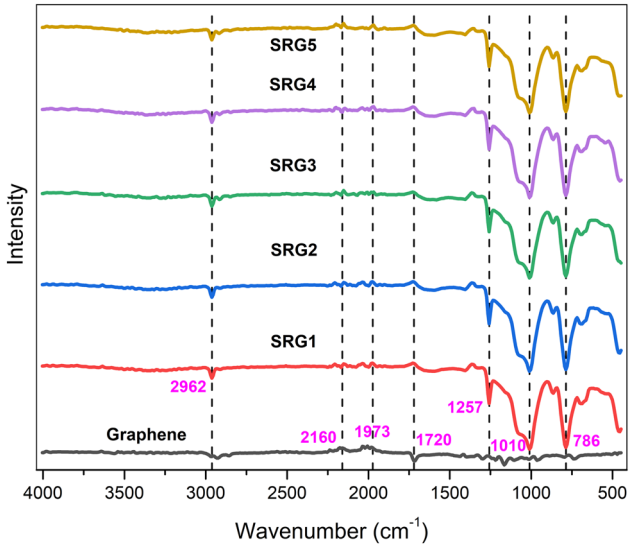

Figure 3: FTIR spectrums of graphene and all nanocomposite samples.

carboxyl group in the graphene molecule at wavenumber 1,720 in addition to the Si bonds.

3.2 Conductivity and dielectric properties

The VNA is used to analyse the SR reinforced with multi-walled graphene's dielectric properties between 1 MHz and 1 GHz. The frequency dependence of conductivity for various compositions is shown in Figure 4(a). It has been demonstrated that as the filler content rises, so does the AC conductivity. Figure 4a illustrates a significant increase in conductivity for the SRG3 (3 wt%) graphene composition. This indicates that the SRG percolation threshold is 3% graphene by weight. The most significant increase in conductivity is seen in the SRG5 composition with a 7% graphene loading, measuring 2.26×10^{-3} S/cm. The formation of conductive network results in the transport of electrons

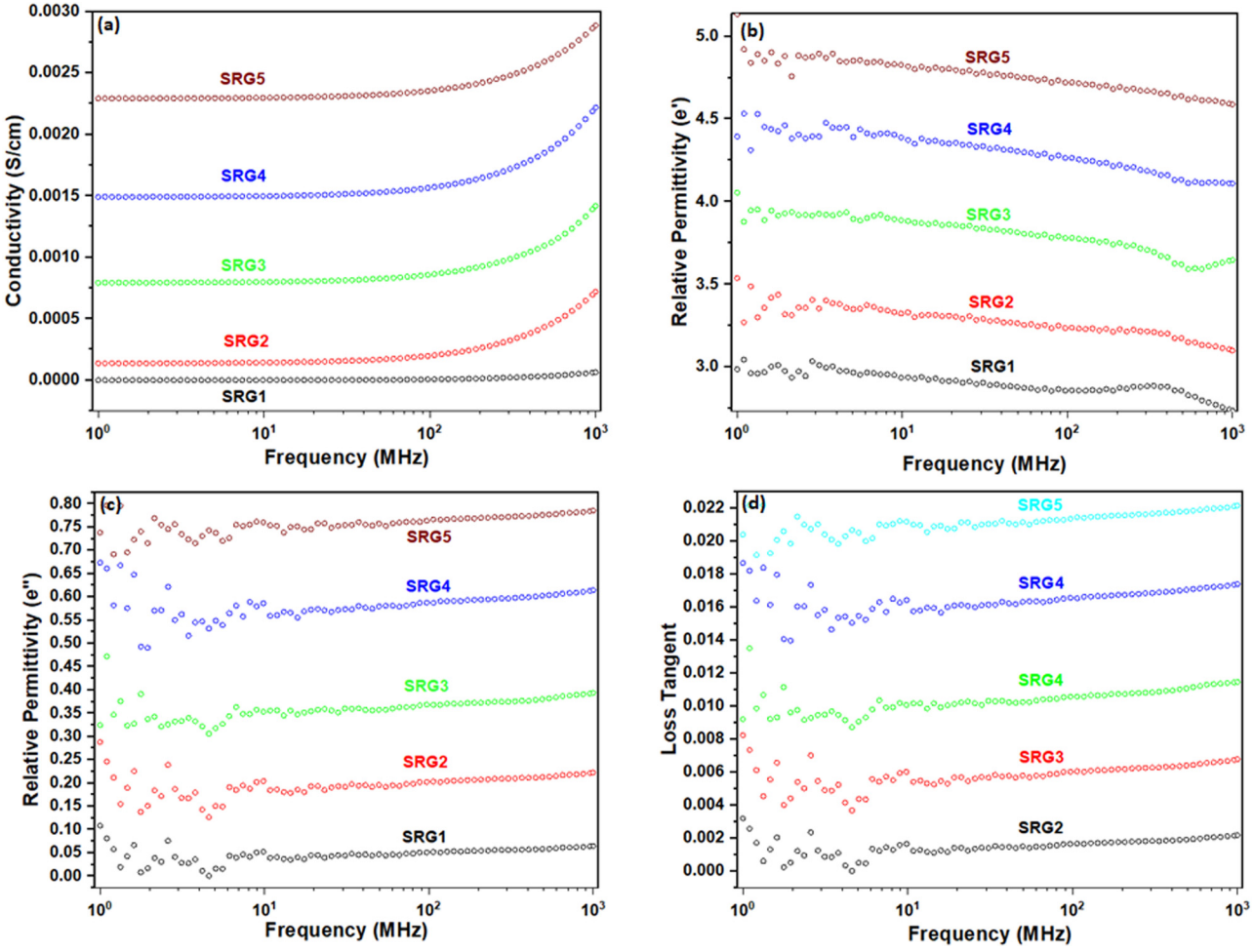

Figure 4: (a) Conductivity; (b) complex permittivity real part (ε'); (c) complex permittivity imaginary part (ε''); and (d) dielectric loss tangent ($\tan\delta$) *vs* frequency.

because of the dense population of graphene [12]. Conductivity is additionally increased by graphene's high aspect ratio and efficient dispersion. At 1 GHz, the SRG1 composition's conductivity is close to zero, while the SRG5 composition's conductivity rises to 2.98×10^{-3} S/cm.

Dielectric permittivity is the measure of a material's capacity to store electric charge, hence a greater value of permittivity indicates a greater capacity to store electric charge. Understanding the EMI SE performance of the material requires this feature. The real (ε') and imaginary (ε'') components of the permittivity are each shown in Figure 4(b and c), respectively. It is clearly demonstrated that both permittivity components get better when graphene content increases. With the increase in the graphene content, Figure 4c shows a further increase in the loss tangent. Compared to pure SR, the ε' and ε'' values for the SRG2 sample increase by about 10–15% (SRG1). ε', which is 5@ 1 MHz for a 7% graphene (SRG5) sample, is shown to increase with the increase in graphene content. The free charge carriers cause graphene's Maxwell–Wagner–Sillar (MWS) effect. This causes interfacial and electronic polarisation and increases the relative permittivity as the amount of graphene increases [19]. The ε' increases as graphene's weight percentage crosses the percolation barrier. This causes the SR/graphene interphases to rise, thereby raising the interfacial polarisation. The MWS effect indicates that the permittivity dramatically increases as the charge accumulates at the contact [20,21].

The ε'' is linked to energy loss in the case of conductive materials. With an increase in the graphene content, ε'' is consistently seen to rise, with SRG5 exhibiting the most significant rise. This may support creating a graphene conductive network and the homogeneous dispersion of graphene throughout the rubber matrix. For SRG1 composition, the dielectric loss ε'' is 0.05@1 MHz, while it rises to 0.075@1 MHz for SRG5 composition. The absorption mechanism of the graphene percolation network produces a higher EM wave dissipation. The loss tangent of

various compositions varies as a function of frequencies, as illustrated in Figure 4(d). The loss tangent has a similar pattern to the imaginary permittivity part. The frequency of SRG1 composition is around 0.01@1 MHz, while the frequency of SRG5 composition is approximately 0.022@1 MHz. As seen in the SEM images, the increased graphene content forms a conductive network that enhances the loss tangent of the SRG4 and SRG5 samples. The increased density of graphene expedites fillers' contact and manifests the network [22].

3.3 EMI SE

The SE [23], expressed as a logarithmic ratio of incident power to transmitted power, is a unit of measurement. EMI SE is mainly influenced by the material's conductivity and dielectric properties, excluding thickness and frequency [24]. This could be achieved by adding conductive nano fillers like graphene to the rubber matrix.

After electromagnetic waves enter a material, their three main impacts are reflection, absorption, and multiple reflections. If the shielding material is conductive, incident EM waves are reflected by the free electrons available at the surface. The loss of waves occurs when electromagnetic waves interact with electric dipoles due to this absorption. It is also important to note that the third element, numerous reflections, is completely disregarded when SE is higher than 10 dB [25].

$$\text{Total SE}_T\ (\text{dB}) = \text{SE}_R + \text{SE}_A, \tag{1}$$

where SE_R is SE due to the reflected component, and SE_A SE is the absorbed component.

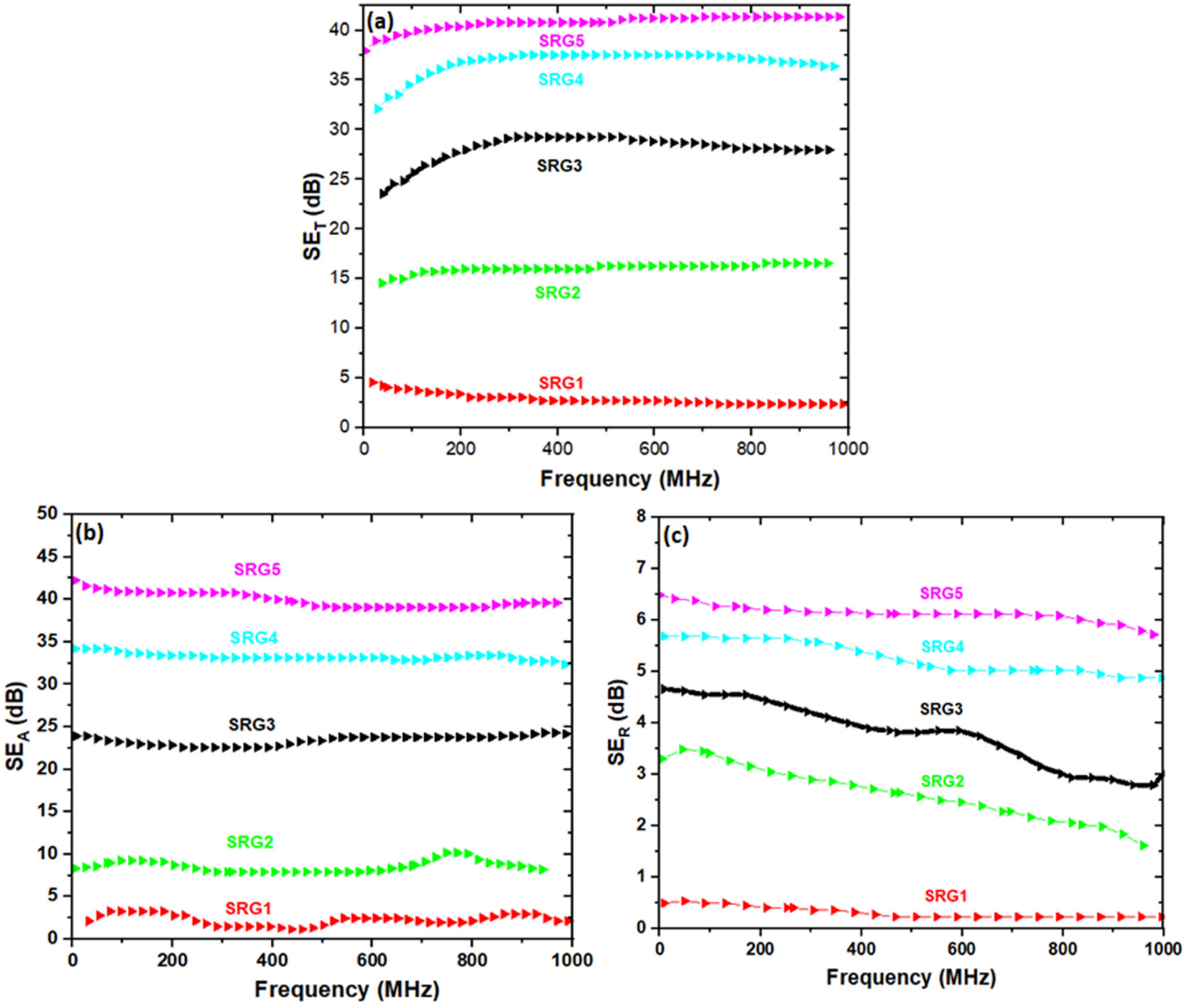

Figure 5: SE in the range of 1 MHz to 1 GHz: (a) total SE_T; (b) absorption SE_A; and (c) reflection SE_R.

Equations (2) and (3) give the SE by absorption (SE_A) and reflection (SE_R) loss, where S_{11} and S_{12} scattering parameters are measured using a VNA [26].

$$SE_A = -10\log\frac{(S_{12})^2}{(1 - S_{11})^2}, \quad (2)$$

$$SE_R = -10\log(1 - S_{11}{}^2). \quad (3)$$

As previously demonstrated, graphene's conductivity and dispersion in the SR matrix are crucial to SE. Since the suggested nanocomposites exhibit superior conductivity and dielectric properties with a rise in graphene weight percentage, improved EMI SE performance is anticipated. Realistic applications must meet EMI SE criteria of 20 dB, or 1% transmittance.

The shielding mechanism is crucial for the materials to be employed for shielding purposes. Figure 5(a)–(c) demonstrate, respectively, the variation in total (SE_T), absorption (SE_A), and reflection (SE_R) SE concerning change in frequency. The sum of the SEs from absorption and reflection is the SE (SE_T). The figure shows that the absorption component is more important than the reflection component. Over the whole frequency range, the SE_A and SE_R for SRG1 composition are between 1.9 and 2.9 dB and 0.22 dB, respectively. With SRG5 composition, the SE_A and SE_R values can reach as high as 39.6 and 6.52 dB, respectively, for the same frequency range. The conducting interfaces expedite numerous reflections causing more excellent SE_A component [27]. The high aspect ratio and conductive network due to the addition of graphene filler are responsible for the multiple reflections. These internal surfaces reduce the energy of EM waves and, in turn, their absorption. Notably, the SE_A is almost constant for all compositions over the whole frequency range. However, when the frequency rises, SE_R tends to fall. The suggested nanocomposite material is suitable for EMI shielding applications in the 1 MHz to 1 GHz frequency range since the SE is more significant than 20 dB and the SE_T is steady over the whole frequency range.

The effects of various compositions on conductivity and EMI SE are depicted in Figures 6(a) and (b). Comparing the two charts reveals that EMI SE rises as conductivity rises. At frequencies of 1 MHz and 1 GHz, the EMI SE is 3.63 and 0.74 dB, respectively, while the conductivity of the SRG1 composition is close to zero. With the increase in graphene loading in the SRG5 composition, EMI SE rises and peaks at 32.94 dB at 1 MHz and 43.22 dB at 1 GHz for a total EMI SE of 32.94 dB. Due to its impact on EMI SE, graphene's physical characteristics, including surface area, aspect ratio, and the availability of extra atoms on top, may be explained. Free electrons are more readily available when graphene's weight percentage increases, which enhances conductivity and SE.

3.4 Simulation of EMI SE

The HFSS model was made to test and understand how different SR/graphene compositions block EMI. Figure 7 illustrates how the model simulation sheds light on how electromagnetic waves propagate through various compositions. Ansys HFSS simulates an experimental set-up like the one used to measure *S* parameters. For the frequency range of 1–3 GHz, a WR510 waveguide is simulated.

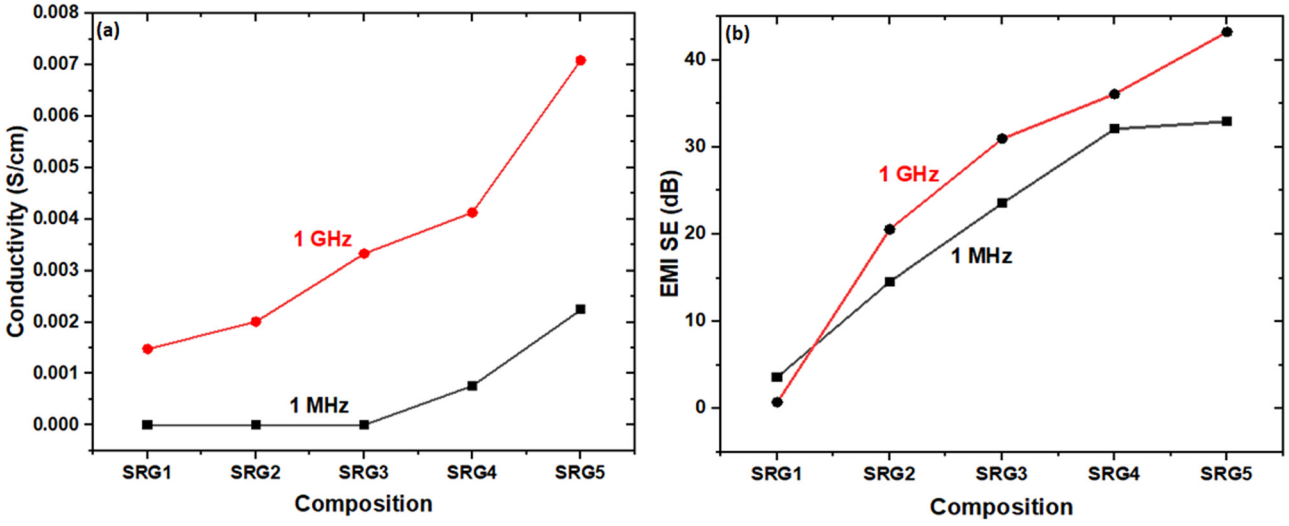

Figure 6: Change in (a) conductivity and (b) SE with the change in weight percentage of graphene.

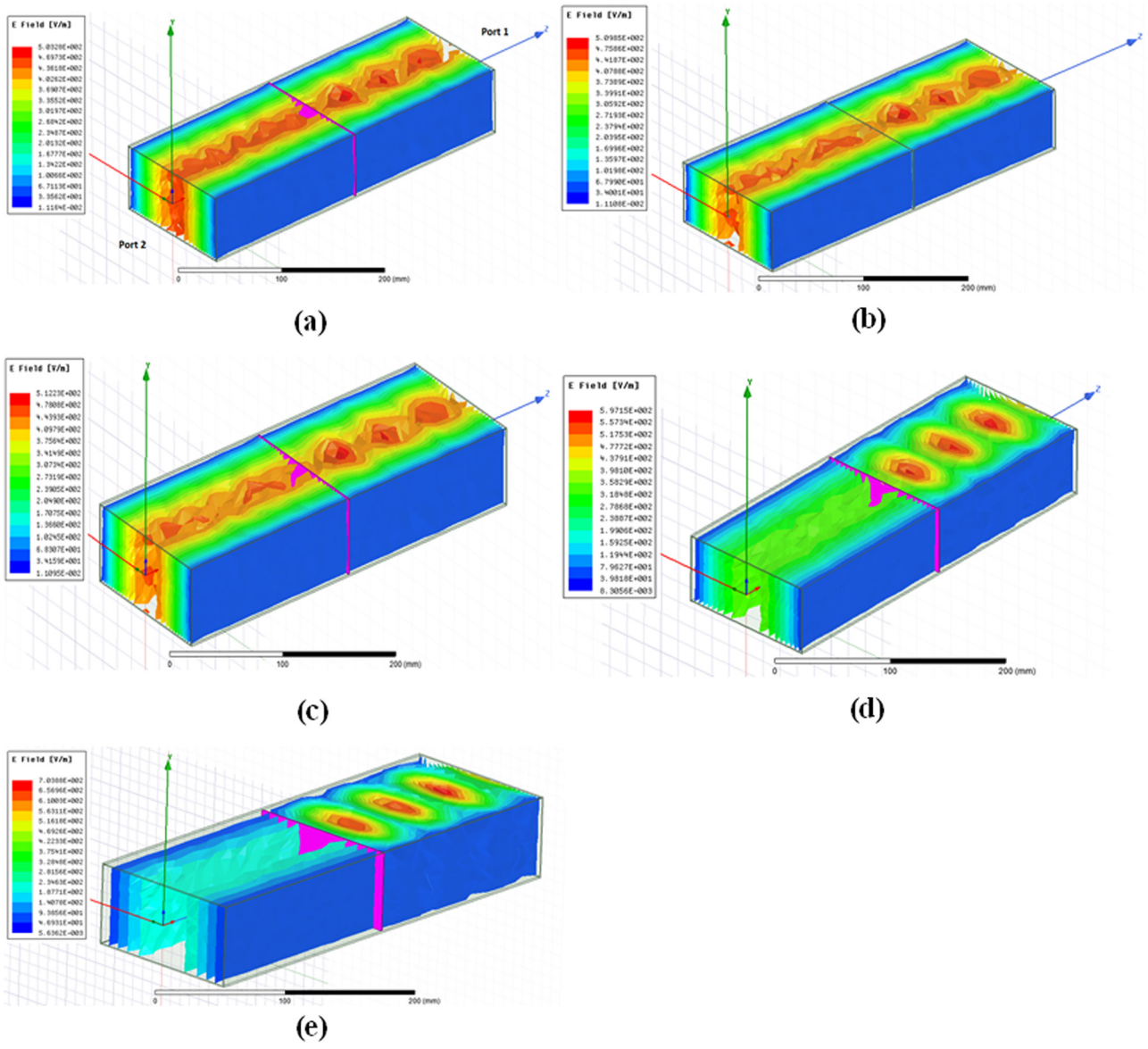

Figure 7: Complex Mag E plots from HFSS simulation of SRG compositions for WR510 waveguide frequency range 1–3 GHz: (a) SRG1, (b) SRG2, (c) SRG3, (d) SRG4, and (e) SRG5.

Air is the transmission medium inside the wave port. Since a wave port excitation is possible in the HFSS, it is applied to S1 (port 1) and S2 (port 2). Transverse electrical excitation is generated at Port 1 and received at Port 2. In the centre of the waveguide, a shielding plate that is 1 mm thick is created. The measured dielectric properties from the experiments are transferred to the shielding plate. 0.1 GHz is the simulated frequency step.

An SR plate consisting of SRG1, a pure SR composition, is shown in Figure 7 to be penetrated by electromagnetic waves. Additionally, there is virtually no difference in the EM field intensity between ports S_1 and S_2. Experimental findings show that the SRG1 composition has a lower standard deviation and poorer electromagnetic wave attenuation (SE). The use of graphene increased the composite's conductivity and changed the path along which the EM energy and EM field propagate. Despite more uniformly distributed magnetic fields, electric field is more potent in the centre than at the edges.

The strength of the electric and magnetic fields is significantly decreased with a graphene loading of 5%, indicating an increase in shielding efficiency (36 dB). The electric and magnetic fields were virtually minimised by the SRG5 composition (7 wt% loadings). This is due to the conductor network in the SRG5 composition. The fact that none of the compositions is affected by the EM waves'

magnetic field is significant because it demonstrates how little magnetic loss there is where the plates and waves meet. The attenuation is caused by reflection and absorption losses, consistent with the experimental results.

4 Conclusion

Using a technique called "compression moulding," the SR/graphene nanocomposite was made, and its dielectric and EMI SE performance was measured. The formation of a percolation network in graphene gives rise to the material's outstanding dielectric properties. It has been established that 3 wt% of graphene is required to exceed the percolation threshold (SRG3 composition). The increase in SR–graphene interactions leads to a rise in interfacial polarisation. Due to the increase in graphene concentration, the dielectric and EMI SE performance improvement within the frequency range of 1 MHz to 1 GHz is noticed. For a sample that is 1 mm thick, the EMI SE of the SRG5 composition varies from 32.94 to 43.22 dB as the frequency changes from 1 MHz to 1 GHz. It has been found that the absorption mechanism makes up most of the entire EMI SE. As proven by experiments, the HFSS simulation of the EM waves validates and supports the composite's performance. This study is easily adaptable and potentially successful in the commercial sphere because it offers the adoption of a straightforward rubber processing approach for manufacturing the nanocomposite for EMI SE applications.

Acknowledgments: The authors wish to thank the Centre for Composite Materials, Kalasalingam University, for the permission to carry out the present research. The authors would also like to thank the Department of Aerospace Engineering, Faculty of Engineering, Universiti Putra Malaysia and Laboratory of Bio-composite Technology, Institute of Tropical Forestry and Forest Product (INTROP), Universiti Putra Malaysia (HICOE) for the close collaboration in this research.

Funding information: The authors would like to thank the Universiti Putra Malaysia for the financial support through Geran Inisiatif Putra Siswazah (GP-IPS) with grant number [9739200].

Author contributions: Avinash Shinde: research and data collection, and drafting the article; Irulappasamy Siva: conception and design of the work, and supervision; Yashwant Munde: data analysis; Irulappasamy Sankar: data analysis and interpretation, and supervision; Mohamed Thariq Hameed Sultan: critical revision of the article and funding acquisition; Farah Syazwani Shahar: data analysis and critical revision of the article; Milan Gaff: data analysis and funding acquisition; David Hui: critical revision of the article and funding acquisition. All authors have accepted responsibility for the entire content of this manuscript and approved its submission.

Conflict of interest: David Hui, who is the co-author of this article, is a current Editorial Board member of *Nanotechnology Reviews*. This fact did not affect the peer-review process. The authors declare no other conflict of interest.

Data availability statement: The datasets generated during and/or analysed during the current study are available from the corresponding author on reasonable request.

References

[1] Saadeh H, Al Fayez RQ, Al Refaei A, Shewaikani N, Khawaldah H, Abu-Shanab S, et al. Smartphone use among university students during COVID-19 quarantine: An ethical trigger. Front Public Health. 2021;9(July):1–11.

[2] Hardell L, Koppel T, Carlberg M, Ahonen M, Hedendahl L. Radiofrequency radiation at Stockholm central railway station in Sweden and some medical aspects on public exposure to RF fields. Int J Oncol. 2016;49(4):1315–24.

[3] Koppel T, Vilcane I, Tint P. Risk management of magnetic field from industrial induction heater - A case study. Eng Rural Dev. 2017;16:1024–37.

[4] Jeddi J, Katbab AA, Mehranvari M. Investigation of microstructure, electrical behavior, and EMI shielding effectiveness of silicone rubber/carbon black/nanographite hybrid composites. Polym Compos. 2019;40(10):4056–66.

[5] Kong LB, Li ZW, Liu L, Huang R, Abshinova M, Yang ZH, et al. Recent progress in some composite materials and structures for specific electromagnetic applications. Int Mater Rev. 2013;58(4):203–59.

[6] Hu YJ, Zhang HY, Li F, Cheng XL, Chen TL. Investigation into electrical conductivity and electromagnetic interference shielding effectiveness of silicone rubber filled with Ag-coated cenosphere particles. Polym Test. 2010;29(5):609–12.

[7] Bregman A, Michielssen E, Taub A. Comparison of experimental and modeled EMI shielding properties of periodic porous xGNP/PLA composites. Polym (Basel). 2019;11(8):1233.

[8] Song P, Song J, Zhang Y. Stretchable conductor based on carbon nanotube/carbon black silicone rubber nanocomposites with highly mechanical, electrical properties and strain sensitivity. Compos Part B Eng. 2020;191(March):107979.

[9] Kong J, Tong Y, Sun J, Wei Y, Thitsartarn W, Jayven CCY, et al. Electrically conductive PDMS-grafted CNTs-reinforced silicone elastomer. Compos Sci Technol. 2018;159:208–15.

[10] Wang R, Yang H, Wang J, Li F. The electromagnetic interference shielding of silicone rubber filled with nickel coated carbon fiber. Polym Test. 2014;38:53–6.
[11] Luan W, Wang Q, Sun Q, Lu Y. Preparation of CF/Ni-Fe/CNT/silicone layered rubber for aircraft sealing and electromagnetic interference shielding applications. Chin J Aeronaut. 2021;34(10):91–102.
[12] Joseph N, Janardhanan C, Sebastian MT. Electromagnetic interference shielding properties of butyl rubber-single walled carbon nanotube composites. Compos Sci Technol. 2014;101:139–44.
[13] Kato Y, Horibe M, Ata S, Yamada T, Hata K. Stretchable electromagnetic-interference shielding materials made of a long single-walled carbon-nanotube-elastomer composite. RSC Adv. 2017;7(18):10841–7.
[14] Morari C, Balan I, Pintea J, Chitanu E, Iordache I. Electrical conductivity and electromagnetic shielding effectiveness of silicone rubber filled with ferrite and graphite powders. Prog Electromagn Res M. 2011;21(September):93–104.
[15] Li Y, Li C, Zhao S, Cui J, Zhang G, Gao A, et al. Facile fabrication of highly conductive and robust three-dimensional graphene/silver nanowires bicontinuous skeletons for electromagnetic interference shielding silicone rubber nanocomposites. Compos Part A Appl Sci Manuf. 2019;119(December 2018):101–10.
[16] Wang G, Liao X, Yang J, Tang W, Zhang Y, Jiang Q, et al. Frequency-selective and tunable electromagnetic shielding effectiveness via the sandwich structure of silicone rubber/graphene composite. Compos Sci Technol. 2019;184(October):107847.
[17] Shen J, Yao Y, Liu Y, Leng J. Preparation and characterization of CNT films/silicone rubber composite with improved microwave absorption performance. Mater Res Express. 2019;6(7):075610.
[18] Ji J, Ge X, Pang X, Liu R, Wen S, Sun J, et al. Synthesis and characterization of room temperature vulcanized silicone rubber using methoxyl-capped MQ silicone resin as self-reinforced cross-linker. Polymers (Basel). 2019;11(7):1142.
[19] Zhai Y, Wu W, Zhang Y, Ren W. Enhanced microwave absorbing performance of hydrogenated acrylonitrile-butadiene rubber/multi-walled carbon nanotube composites by *in situ* prepared rare earth acrylates. Compos Sci Technol. 2012;72(6):696–701.
[20] Abraham J, Mohammed Arif P, Kailas L, Kalarikkal N, George SC, Thomas S. Developing highly conducting and mechanically durable styrene butadiene rubber composites with tailored microstructural properties by a green approach using ionic liquid modified MWCNTs. RSC Adv. 2016;6(39):32493–504.
[21] Abraham J, Arif PM, Xavier P, Bose S, George SC, Kalarikkal N, et al. Investigation into dielectric behaviour and electromagnetic interference shielding effectiveness of conducting styrene butadiene rubber composites containing ionic liquid modified MWCNT. Polymer (Guildf). 2017;112:102–15.
[22] Gao Y, Wang C, Li J, Guo S. Adjustment of dielectric permittivity and loss of graphene/thermoplastic polyurethane flexible foam: Towards high microwave absorbing performance. Compos Part A Appl Sci Manuf. 2019;117(June 2018):65–75.
[23] Arjmand M, Apperley T, Okoniewski M, Sundararaj U. Comparative study of electromagnetic interference shielding properties of injection molded versus compression molded multi-walled carbon nanotube/polystyrene composites. Carbon N Y. 2012;50(14):5126–34.
[24] Dhakate SR, Subhedar KM, Singh BP. Polymer nanocomposite foam filled with carbon nanomaterials as an efficient electromagnetic interference shielding material. RSC Adv. 2015;5(54):43036–57.
[25] Li N, Huang Y, Du F, He X, Lin X, Gao H, et al. Electromagnetic interference (EMI) shielding of single-walled carbon nanotube epoxy composites. Nano Lett. 2006;6(6):1–5.
[26] Joseph N, Sebastian MT. Electromagnetic interference shielding nature of PVDF-carbonyl iron composites. Mater Lett. 2013;90:64–7.
[27] Sang G, Dong J, He X, Jiang J, Li J, Xu P, et al. Electromagnetic interference shielding performance of polyurethane composites: A comparative study of GNs-IL/Fe_3O_4 and MWCNTs-IL/Fe_3O_4 hybrid fillers. Compos Part B Eng. 2019;164(January):467–75.